Achieving structural rejuvenation in metallic glass by modulating β relaxation intensity via easy-to-operate mechanical cycling

L.T. Zhang[a], Y.J. Wang[b,c], E. Pineda[d], Y. Yang[e,f], J.C. Qiao[a,g*]

[a]School of Mechanics, Civil Engineering and Architecture, Northwestern Polytechnical University, Xi'an 710072, China

[b]State Key Laboratory of Nonlinear Mechanics, Institute of Mechanics, Chinese Academy of Sciences, Beijing 100190, China

[c]School of Engineering Science, University of Chinese Academy of Sciences, Beijing 100049, China

[d]Department of Physics, Institute of Energy Technologies, Universitat Politècnica de Catalunya, 08019 Barcelona, Spain

[e]Department of Mechanical Engineering, College of Engineering, City University of Hong Kong, Tat Chee Avenue, Kowloon Tong, Kowloon, Hong Kong SAR, China

[f]Department of Materials Science and Engineering, College of Engineering, City University of Hong Kong, Tat Chee Avenue, Kowloon Tong, Kowloon, Hong Kong SAR, China

[g]Innovation Center, NPU-Chongqing, Chongqing 401135, China

Submitted to International Journal of Plasticity

* Corresponding author: Prof. Dr. J.C. Qiao (qjczy@nwpu.edu.cn)

Abstract

Structural rejuvenation is an effective measure to optimize the mechanical properties of metallic glasses (MGs). Sophisticated solutions to rejuvenation include thermal cycling, laser shocking, and multiaxial stress loading. Here, we propose an easy-to-operate mechanical cycling as an alternative strategy to tailor the mechanical relaxation, deformation, and structural heterogeneity of MGs. Structural rejuvenation in a La-based MG is achieved via mechanical cycling even at very few cycles (10^2 tension load cycles) and low frequencies (10^{-3} Hz). The results manifest intuitively the competition between structural relaxation and rejuvenation, which constitutes the structural evolution in MGs. A theoretical model is constructed which reveals a scenario of that mechanical cycling wakes up frozen flow defect, accelerating creep and, thus, enhancing the β relaxation in MGs. Therefore, this handy anti-ageing methodology supplies an alternative pathway to optimize the mechanical properties of MGs. It also contributes towards a more comprehensive understanding of the structure-property relationship in amorphous materials, especially with regards to the correlation between structural rejuvenation and relaxation behavior in such topologically disordered materials.

Keywords: Metallic glass; Rejuvenation; Mechanical cycling; β relaxation; Anelasticity

1. Introduction

Metallic glasses (MGs) have gained the favor of materials science and condensed matter physics due to their excellent mechanical and functional properties (Ashby and Greer, 2006; Johnson, 1986; Qiao et al., 2019; Qiao et al., 2022; Rao et al., 2022; Wang, 2019). Unfortunately, they frequently fail in a brittle manner, in particular, at tensile loading and, therefore, cannot be plastically deformed at room temperature in their bulk form. The disadvantage in tensile ductility presents a major bottleneck for applications as structural materials (Chen and Dai, 2016; Chen et al., 2013; Greer et al., 2013; Zhang et al., 2022). MGs are usually formed by rapidly cooling a melting liquid. Higher cooling rate fabricates more disordered and thermodynamically metastable glasses. Physical aging (even at room temperature) introduces structural relaxation of MGs towards a more stable energetic state and thereby deteriorating a number of their initial properties such as plasticity and limiting their widespread applications. The reverse process to structural relaxation, termed rejuvenation, is desired and attractive because it allows MGs to go back to higher-energy and less brittle state (Ding et al., 2019; Greer and Sun, 2016; Ketov et al., 2015; Lacks and Osborne, 2004; Pan et al., 2020; Pan et al., 2018; Sun et al., 2016). Despite these great achievements, the existing rejuvenation strategies usually suffer from technical complexity. Therefore, an easy-to-operate method in laboratory to structurally rejuvenate the MGs urgently needs in-depth studies. The way to achieve rejuvenation is of great scientific and technological importance, because it determines physical properties of MGs. Ketov et al. reported that via cyclic cryogenic process, the rejuvenation of the glass can be achieved by the introduction of the non-affine strains, leading to a recovery of relaxation enthalpy and an enhancement of the room-temperature plasticity (Ketov et al., 2015). As a matter of fact, stress plays an equivalent role as temperature in glass dynamics, which indicates that the yield of MGs can be regarded as a stress-driven glass transition (Guan et al., 2010). The reveal of such a stress-temperature scaling promotes the development of stress-induced rejuvenation in MGs. It has been demonstrated in literature that stress-induced rejuvenation by activating shear transformation events introduces more flow defects

into MGs and can be divided into the cold working and hot working (Sun et al., 2016). Severe plastic deformation induced by the cold working including uniaxial compression, cold rolling, and high-pressure torsion has the potential to considerably rejuvenate MGs (Sun et al., 2016). On the other hand, hot working like thermo-mechanical creep can achieve rejuvenation when the magnitude of stress exceeds a threshold value (Tong et al., 2018). Additionally, the structural change by thermo-mechanical creep is largely associated with anelastic strain (Tong et al., 2015). It is worthy to note that mechanical cycling has been comprehensively studied by molecular dynamics simulations of model atomic glasses. Cycling the strain ultimately leads to a steady state. Whether the glass is relaxed or rejuvenated depends on the initial state (Fiocco et al., 2013). It can expected that the MGs returns to the same energy minimum at the end of each cycle in the situation of low amplitude strain (Fiocco et al., 2014). Work hardening has been reported in the cyclic nanoindentation loading (Packard et al., 2010). Recently, Ross et al. reported that fatigue subjected to 10^6 compressive load cycles at a rate of 10 Hz with a maximum stress of $0.43\sigma_y$ (σ_y is the yield stress) promotes the formation of local high-energy states of an MG (Ross et al., 2017).This result opens the door of rejuvenation of MGs via mechanical cycling and encourages us to explore the nature of structural rejuvenation upon this strategy. Notably, rejuvenation upon such amounts of cycles and high frequency at room temperature still deserves improvenment. It is imperative to explore how mechanical cycling rejuvenates MGs and whether significant rejuvenation could still be achieved with fewer cycles and lower frequencies. Moreover, we would like to emphasize that structural relaxation is accelerated by increasing the ambient temperature; thus, there is a competition between structural relaxation and rejuvenation during mechanical cycling. In other words, this is a vital matter that must be overcome to achieve rejuvenation via mechanical cycling. If optimized (in terms of temperature, frequency and amplitude), mechanical cycling holds a great and largely unexplored potential for accessing new rejuvenated states. Indeed, the fact that the MGs may show a rejuvenation via mechanical cycling is a fascinating possibility.

Ambient temperature, which ultimately determines the thermodynamic state or potential energy of MGs, takes a vital role in various rejuvenation methods as

mentioned above. To some extent, the ambient temperature also determines the occurrence of relaxation events, i.e., boson peak, γ relaxation, slow β relaxation, and α relaxation, etc. As reported by Ding et al., with heavier rejuvenation, the boson peak becomes stronger and moves to lower temperatures (Ding et al., 2019). At the same time, the activation of γ relaxation of MGs also causes a remarkable loading frequency-dependent enthalpy storage and has been demonstrated as a universal phenomenon (Küchemann and Maaß, 2017). In our previous work, we have shown an unexpected decoupling of the relaxation mechanism below the glass transition temperature into a fast stress-driven and a slow thermally activated mode, which also provides convincing evidence that the rejuvenation is controlled by the specific mode and intensity of mechanical relaxation (Qiao et al., 2016). This in turn leads to intriguing questions: is it possible to achieve rejuvenation by modulating the β relaxation, and what is the correlation between β relaxation and rejuvenation?

Mechanical spectroscopy is a key experimental technique for investigating atomic rearrangements and the mechanical relaxation behaviors of MGs, and has been widely employed to obtain fundamental physical parameters such as storage modulus, loss modulus and internal friction, etc., guiding the exploration of the atomic rearrangements underlying the stress-assisted and thermally activated processes (Qiao et al., 2019; Wang, 2019). Benefitting from these advantages, mechanical spectroscopy was widely used to probe the relaxation processes of MGs. MGs actually show two main relaxation kinetics processes, which are called main α relaxation and secondary β relaxation (also named Johari-Goldstein, JG relaxation) (Johari and Goldstein, 1970). The α relaxation, viewed as large-scale irreversible rearrangement of atoms, is connected with the dynamic glass transition and viscous flow behavior. On the other hand, the β relaxation process is closely related to locally reversible atomic motion and plastic deformation, which appears at lower temperature or higher frequency. The presence of β relaxations and its relationship to structural heterogeneity in the glass state have been discussed since the earliest works reporting such phenomena (Johari and Goldstein, 1970). However, the debate on their microscopic origin remains

dynamic (Casalini and Roland, 2009; Johari, 2002; Lu et al., 2016; Ngai and Capaccioli, 2004; Tanaka, 2004; Wang et al., 2019; Yu et al., 2012; Yu et al., 2010; Zhu et al., 2016). What is certainly true is that, the β relaxation process is related to unrelaxed structures produced by rapid cooling, and mainstream opinion proposes that they are indicative of structural heterogeneity. While the spectrum of the α relaxation is very similar in all MG systems, the manifestation of β relaxation characterizes the individuality of the distribution of relaxation times of each particular sample (Qiao et al., 2019; Wang, 2019; Yu et al., 2013). In addition, it has been regarded that β relaxation process is linked to the activation of flow defects locally confined in the elastic matrix of MGs, while α relaxation is associated with the percolation of flow defects through the elastic matrix (Harmon et al., 2007; Johnson and Samwer, 2005). There are amounts of investigations which proved the connection between β relaxation process and internal physical and mechanical properties of MGs (Casalini and Roland, 2009; Evenson et al., 2014; Ngai and Capaccioli, 2004; Song et al., 2020; Yang et al., 2020).

The apparently interesting but seemingly unclear findings about rejuvenation of MGs are calling for a systematic investigation on the rejuvenation-relaxation events relationships in MGs. Previous investigations have not yet answered the following questions: Is it possible to achieve considerable rejuvenation upon a few cycles and low frequencies and what controls the rejuvenation during the mechanical cycling process? How to construct a map of competition between rejuvenation and structural relaxation in terms of mechanical cycling intensity and time? How does the rejuvenation tailor the slow β relaxation and to what extent it controls the mechanical performance of a rejuvenated MG? To answer these questions, we recognize that a key step is to obtain insights into the intrinsic correlation between rejuvenation induced by mechanical cycling and the modulation of structural heterogeneity, which has never been thoroughly clarified before.

It is worth noting that many glassy materials exhibit an evident β relaxation, which is closely connected to plasticity (Yu et al., 2013). Investigations demonstrated that several MGs show remarkable β relaxation in the framework of loss modulus E''.

Interestingly, La-based MGs attract attention due to the obvious β relaxation and relatively low glass transition temperature (Wang, 2019). We use established concepts to experimentally probe structural rejuvenation states of a glass with the intention of linking the characteristic parameters from theory to the properties of the MG. The current research attempts to interpret the new insights of the structural rejuvenation of a $La_{30}Ce_{30}Ni_{10}Al_{20}Co_{10}$ MG with pronounced β relaxation via easy-to-operate mechanical cycling. Based on the experimental and theoretical study, the relationship among β relaxation, cyclic deformation and structural rejuvenation in the unique alloy is developed. The results show that our strategy even at very few cycles (10^2 tension load cycles) and low frequencies (10^{-3} Hz) still awakes the frozen flow defects confined in the elastic matrix, creating a rejuvenated glass and improving the structural heterogeneity. A map of competition between structural rejuvenation and physical aging in terms of mechanical cycling intensity and time is also constructed. Last but not the least, the structural indexes of aging and rejuvenation were summarized and discussed in the present framework of rejuvenation enabled by easy-to-operate mechanical cycling.

2. Experimental procedure

2.1 Sample preparation

The master alloy with a nominally chemical atomic composition of $La_{30}Ce_{30}Ni_{10}Al_{20}Co_{10}$ (at %) was prepared by arc-melting pure metals in the high-purity argon atmosphere. In order to scavenge oxidation during the process, a titanium getter was employed. The master alloy was then re-melted at least six times to ensure its chemical homogeneity at medium or long-range length scale. Single-roller melt-spinning technique was used to prepare ribbons with a width of 1.2 mm and a thickness of 30 μm.

2.2 Mechanical cycling

The mechanical cyclic experiments on $La_{30}Ce_{30}Ni_{10}Al_{20}Co_{10}$ MG were performed in a commercial dynamic mechanical analyzer (DMA, TA Q800) in tensile mode at 363

K below T_g (~438 K). During the heating period, we applied a tensile load of 0.01 N in order to reduce the bending of the as-cast ribbon. The very first point that needs to be made, we think, is that the intensity of mechanical cycling is controlled by three parameters, i.e., stress amplitude, stress rate, and mean stress, respectively. The increase in any one of these parameters can effectively improve the intensity of mechanical cycling. As a consequence, the cyclic loading/unloading was finally performed in three modes: (I) At constant stress rate of 50 MPa/min and mean stress of 100 MPa, the stress amplitude ranges from 0 to 150 MPa; (2) At mean stress of 100 MPa and stress amplitude of 100 MPa, the stress rate ranges from 12.5 to 100 MPa/min; (3) At constant stress rate of 50 MPa/min and stress amplitude of corresponding mean stress, the mean stress ranges from 25 to 200 MPa. These three modes were repeated for 8 h for one complete set of cycle. A representative example of a subset of the 120 cycles is shown in **Fig. 1(a)**.

2.3 Dynamic mechanical relaxation

The storage and loss moduli of the glassy ribbons were measured by DMA using the tension film configuration. Under a simulation of sinusoidal stress $\sigma = \sigma_0\cos(2\pi f t)$, the strain response of a typical viscous elastic material can be monitored as $\varepsilon = \varepsilon_0\cos(2\pi f t + \delta)$, where f is the loading frequency and δ the phase lag. The complex Young's modulus can be expressed as $E = \sigma/\varepsilon = E' + iE''$ in the complex plane, where E' and E'' are the storage and loss moduli, respectively. The mechanical relaxation spectra were determined by heating the glassy ribbons with mechanical cycling treatment at testing frequencies of 1, 2, 4, and 8 Hz and heating rate of 2 K/min. **Fig. 1(b)** shows the evolution of the normalized storage modulus E'/E_u and loss modulus E''/E_u at testing frequency of 4 Hz and heating rate of 2 K/min, where E_u is the value of the storage modulus at ambient temperature. We can see that E'/E_u almost decreases linearly with increasing temperature while a pronounced peak domains the E''/E_u curve.

3. Results and discussion

3.1 Effect of mechanical cycling on creep

In a closed system, the adsorbed thermal energy (ΔQ) and the input mechanical energy (W) into constant volume are in balance with the change of the internal energy (ΔU), which is the first law of thermodynamics. In mechanical cycling, most of the input mechanical energy is recovered when the load is released, which is attributed to the elastic component of deformation. However, a fraction of the input mechanical energy is dissipated and becomes irrecoverable (W_{diss}) due to the inelastic deformation. It changes the internal energy of the system and dissipates the self-generated thermal energy. Therefore, applied cyclic loading on a specimen is understood as an irreversible thermodynamic process and, thus, the law of the conversation of energy can be formulated as follows:

$$W_{diss} = \Delta U + \Delta Q \tag{1}$$

In addition, the concept of strain energy density $\nu_{\varepsilon} = \sigma\varepsilon$ is introduced. In the tensile loading experiments at the stress ratio $\sigma_{max}/\sigma_{min}$ of 1.0, the total energy dissipation ν_{ε_total} was attributed purely to creep and therefore was set equal to ν_{ε_creep}. At the stress ratio of −1.0, the origin of the energy dissipation was attributed to pure cyclic loading and then ν_{ε_total} was set equal to ν_{ε_cyclic}. Generally, ν_{ε_total} was set equal to the sum of ν_{ε_cyclic} and ν_{ε_creep} at other stress ratios, as follows:

$$\nu_{\varepsilon\_total} = \nu_{\varepsilon\_cyclic} + \nu_{\varepsilon\_creep} \tag{2}$$

ν_{ε_cyclic} was defined by the summation of all the individual stress-strain hysteresis areas measured throughout the loading time of the specimen, as follows:

$$\nu_{\varepsilon\_cyclic} = \sum_{i=1}^{n} \nu_{\varepsilon\_cyclic,i} \tag{3}$$

where $\nu_{\varepsilon\_cyclic,i}$ denotes the hysteresis area per cycle for the ith cycle, and n is the number of cycles. Alternatively, ν_{ε_cyclic} was obtained here by calculating the area

under the graph of $\nu_{\varepsilon\_cyclic,i}$ versus n from the first to the last cycle. ν_{ε_creep} was defined by the summation of all the mean stress strain areas as follows:

$$\nu_{\varepsilon\_creep} = \sigma\varepsilon\_creep \quad (4)$$

To be more specific, **Fig. 2** displays the schematic representation of the hysteresis loops during a pure cyclic loading and the stress-strain curve during a pure creep test. The dash area corresponds to ν_{ε_cyclic} and ν_{ε_creep}. **Figs. 3(a)-(c)** shows the time development of the system strain at varying stress amplitude, stress rate, and mean stress, respectively. All curves show the classical behavior of two-stage strain evolution. The initial period of strain establishment and its spatial distribution, consisting of a steep increase followed by a gradual approach to saturation, is known as primary or transient creep. The secondary stage of steady-state creep is a period of linear strain increase in time. The extent of this stage depends on the combination of the system temperature, mean stress, stress rate, and stress amplitude. The strain and strain rate increase gradually with further increasing the stress amplitudes, confirming a signal that mechanical cycling can accelerate the deformation processes. In addition, the results unambiguously indicate that the flow defects in the samples become active even at a stress far less than the yield strength. The experimental results also show that the strain and strain rate increase with increasing stress amplitude/stress rate/mean stress, indicating a larger volume fraction of atoms in the matrix is activated and transforms into soft regions. Based on Eqs. (2)~(4), the time development of ν_{ε_creep}, ν_{ε_total}, and $\nu_{\varepsilon\_creep}/\nu_{\varepsilon\_total}$ at varying stress amplitude, stress rate, and mean stress are displayed in **Figs. 3(d)-(l)**. From the results, the following observation can be made: (i) Reasonable trend shows that ν_{ε_creep} and ν_{ε_total} increase monotonically with increasing stress amplitude/stress rate/mean stress; (ii) With the increase of the stress amplitude or stress rate, ν_{ε_cyclic} plays a more important role in ν_{ε_total} but a less important role acted by increasing the mean stress, which indicates the former may possess a high value of cyclic deformation; (iii) At a first glance, ν_{ε_creep} increases

linearly with time in the secondary stage, where the strain rate approximately reaches at a constant value. On the other hand, ν_{ε_total} exhibits a slope and smooth time which are apparently different from that of ν_{ε_total}, which is attributed to the saturation time and steady-state strain rate of creep and cyclic loading.

Recently, a number of studies described the relaxation locally based on the concept of flow defects which are associated with the dynamic heterogeneities, as well as energy and density fluctuations (Dmowski et al., 2010b; Kosiba et al., 2019; Qiao et al., 2019; Ye et al., 2010), such as the quasi-point defect (QPDs) theory (Perez, 1990) or flow units (Wang and Wang, 2019). Besides, it seems very promising, to correlate glass properties to the "soft region" or "flow defects" parameter. The structure of MGs is intrinsically heterogeneous from a dynamic point of view, being composed of liquid-like and solid-like regions at the nanoscale. Such a "core-shell' model, which consists of a free-volume zone and its surrounding elastic matrix, captures the basic topological feature of the atomic structure of MGs (**Fig. 4(a)**). In the model, the "core" region, i.e., the soft region with loosely packed atomic structure and high fraction of free volume, can be more easily activated during plastic deformation to act as the "flow defects". The microscopic mechanism of the deformation in MGs can be rationalized by the "core" region with a characteristic relaxation time τ_1 and "shell" region with τ_2 (**Fig. 4(b)**).

We present the mechanical data as the ratcheting creep deformation (ratcheting is the buildup of anelastic strain with asymmetric cycling deformation). The ratcheting creep strain $\varepsilon_{\text{creep}}$ is defined as:

$$\varepsilon_{\text{creep\_cycle}} = \frac{\varepsilon_{\text{max\_cycle}} + \varepsilon_{\text{min\_cycle}}}{2} \tag{5}$$

where $\varepsilon_{\text{max\_cycle}}$ and $\varepsilon_{\text{min\_cycle}}$ are the maximum and minimum of strain over each set of cycles. The anelastic flow of a MG often occurs in the elastic region below the yield stress, which is closely related to the non-equilibrium characteristics of amorphous solids. Unlike the plastic flow behavior of MGs, anelastic flow is relatively uniform on the macroscopic scale, generally no shear band propagates (Ye et al., 2010). Typical anelastic flow occurs when MGs are dynamically loaded and unloaded in the elastic

region, and it appears as a hysteresis loop of the stress-strain curve. Hence, the total strain of MGs includes the elastic deformation ε_e, the anelastic deformation ε_{an} and the visco-plastic deformation ε_{vp}. ε_{an} and ε_{vp} gradually increase with increasing stress holding time and eventually reach a saturated state. When the stress is completely released, the elastic part ε_e and the anelastic part ε_{an} completely disappear after sufficiently relaxation time, only remaining the visco-plastic part ε_{vp} (Taub and Spaepen, 1981). The viscoelasto-viscoplastic constitutive models based on the springs and dashpot elements can describe the creep behavior of amorphous materials (Barriere et al., 2020; Hasanpour et al., 2009; Khan and Zhang, 2001). Especially, Khan et al. proposed a model to simulate the nonlinear deformation response of polymers, characterizing the complex and nonlinear mechanical behavior (Khan and Lopez-Pamies, 2002; Khan et al., 2006). Phenomenologically, the anelastic and visco-plastic deformation can be described as a series of linear springs and dashpots, known as the generalized Kelvin model, which is commonly used for describing the creep of MGs, i.e.,

$$\varepsilon = \varepsilon_e + \sum_{i=1}^{n} \varepsilon_i \left(1 - e^{-t/\tau_i}\right) + \dot{\varepsilon}_{vp} t \tag{6}$$

where ε_i is the strain and τ_i is the characteristic relaxation time for the activation of the i-th anelastic process, $\dot{\varepsilon}_{vp}$ is a constant visco-plastic strain rate corresponding to the last dashpot. The two-phase model as proposed in MGs can be characterized by two anelastic relaxation processes during the creep process (Castellero et al., 2008). Therefore, two Kelvin units with a Maxwell unit were chosen to analyze the anelastic and visco-plastic deformation of the studied MG, i.e., n = 2 (as shown in **Fig. 4(c)**). The typical ratcheting creep data at different stress amplitudes can be fitted well by using the Maxwell-Voigt model based on the two-phase hypothesis:

$$\varepsilon = \varepsilon_e + \varepsilon_1 \left(1 - e^{-t/\tau_1}\right) + \varepsilon_2 \left(1 - e^{-t/\tau_2}\right) + \dot{\varepsilon}_{vp} t \tag{7}$$

where ε_1 and τ_1 represent the strain and relaxation time of the first Kelvin unit, ε_2 and τ_2 represent that of the second Kelvin unit, and $\dot{\varepsilon}_{vp}$ is a constant strain rate related to

the Maxwell dashpot. It is seen that structural heterogeneity at the nanoscale as found in many MGs (Yuan et al., 2021) can be precisely described by two characteristic relaxation time τ_1 and τ_2 by using the two-phase model, namely, the glassy matrix that possesses long relaxation time (i.e., large size) will show a relatively high hardness or elastic modulus relating to hard regions, while that with more small defects (short relaxation time) relates to soft regions. The convergence of the present setup in this model in describing the anelastic behaviors of MGs can be verified by the consistence between experimental data and theory. **Figs. 5(a)-(c)** displays the ratcheting strain-time curves simulated by Eq. (7) according to the Maxwell-Voigt model. Good fittings can be observed. It has been suggested that the number, intensity and characteristic relaxation time of the anelastic processes activated during the constant load segment depend on the degree of structural relaxation and the temperature (Castellero et al., 2008; Ocelík et al., 1997). In our case, an interesting feature is the dependence on the mechanical cycling intensity, which is inversely proportional to the structural relaxation. For La-based MG, two anelastic deformation processes are activated during the holding segment at a homologous temperature (T/T_g~0.83). It is interesting to compare this result with that reported in Ref. (Concustell et al., 2006) for Pd-based MG, where only one anelastic deformation process is activated at T/T_g~0.52. It is evident that a larger number of anelastic deformation processes is activated when the experiment is performed at higher normalized temperature. The values of the fitting parameters for the ratcheting creep curves, together with the error due to the fitting procedure, are shown in **Table 1**. Several points can be reached after checking these fitting parameters in different loading protocols: (i) With the increase in stress amplitude, the significant decrease of strain as indicated by ε_1 with increasing stress amplitude can be observed, accompanying the shift of characteristic relaxation time of Kelvin units τ_1 towards a slower time region. However, the values of ε_2 and τ_2 clearly change which are associated with the second anelastic component. While τ_2 decreases significantly for both alloys, ε_2 increases slightly with increasing stress amplitude. This phenomenon demonstrates that more defects with a faster characteristic relaxation time and less

defects with a slower relaxation time are activated under the mechanical cycling mode. Finally, it is noticed that the visco-plastic strain rate progressively increases with increasing stress amplitudes, demonstrating an evident drop of viscosity upon the increase of stress amplitude. (ii) The effect of the stress rate on ratcheting creep is similar to that of stress amplitude, indicating that the equivalency of the stress rate and stress amplitude. (iii) ε_1 and ε_2 both increase significantly with increasing mean stress while τ_1 and τ_2 decrease sharply. As a result, increasing the mean stress is beneficial to activate more defects in core and shell region and accelerate these processes. The ratio of ε_2 to ε_1 was calculated to further clarify the difference among the effect of stress amplitude, stress rate, and mean stress. We can see that $\varepsilon_2/\varepsilon_1$ increases clearly with increasing stress amplitude and rate but shows a negligible dependence on mean stress. This also confirms that pure creep domains the deformation behavior for the high mean stress, as indicated by **Fig. 3(l)**.

According to the Maxwell-Voigt model, the overall anelastic strain can be partitioned into the contribution of the elastic matrix and that of the flow defects. It should be herein emphasized that the flow defects play a more important role in the anelastic deformation with a higher mechanical cycling intensity. In other words, MGs look more like the flow liquid under a higher mechanical cycling intensity.

As proposed in the work of Castellero et al. (Castellero et al., 2008), the relaxation time spectrum based on the Maxwell-Voigt model can accurately describe the two anelastic creep processes of MGs:

$$L(\tau) = K\left[(1 + t/\tau_1)(\varepsilon_1/\tau_1)e^{-t/\tau_1} + (1 + t/\tau_2)(\varepsilon_2/\tau_2)e^{-t/\tau_2}\right]t|_{t=2\tau} \qquad (8)$$

where $L(\tau)$ is the spectrum intensity, K is a constant and equals to $1/\sigma_0\varepsilon_0$. **Figs. 5(d)-(f)** gives the relaxation spectra of the La-based MG. The observed two coupling relaxation peaks in each relaxation spectra are related to the two relaxation processes demonstrated by two characteristic relaxation times τ_1 and τ_2 under the Maxwell-Voigt model. The two different types of processes are most probably connected to different types of heterogeneity in the samples. Both peaks show an increase in intensity and a slight shift towards shorter relaxation times as the increases of the mechanical cycling

intensity; such a trend is more pronounced for the second peak with respect to the first one. It means that more defects with a relatively small size are activated. This phenomenon has also been observed in a CoFe-based MGs, which reveals that more free volume or defect is activated at a higher loading rate (Lv et al., 2021). Castellero et al. correlated the defects with the creep behavior, and they suggest that the reduction of peak intensity and the shift of the peaks to longer relaxation times can be attributed to the decrease of the population of the corresponding defects. Therefore, the activation of the remaining defects becomes more difficult during physical aging (Castellero et al., 2008). In our case, it should be mentioned that the increase of the mechanical cycling intensity makes the activation of defects at both shorter and longer relaxation times easier, which are activated along with the generation of free volumes. It agrees well with previous observation in MG that the excess free volume generated during the creep deformation can be simulated at a high loading rate (Yuan et al., 2021). This process might benefit the propagation of flow defects (Argon, 1979). The superposition of the atomic clusters inside those defects during deformation together with the generation of plenty of free volumes is in favor of a pronounced creep deformation via the homogeneous plastic flow. The correlations among the relaxation spectra derived from creep experiments, the material structure and the deformation mechanism should be paid more attention for understanding the unsolved issues on creep of MGs.

3.2 Effect of mechanical cycling on β relaxation

Despite the mechanical properties, the relaxation dynamics and the deformation behaviors are usually studied by different stress/strain levels, the correlation between them might imply the existence of underlying structure-properties connections. This is a long-standing aim of studies on MGs. It is noted that an important factor to understand the physical properties of MGs is the atomic mobility. Modifications of enthalpy and entropy are induced by various treatments. Atomic mobility could also be modified during the physical aging or plastic deformation in amorphous state. Therefore, the aging or rejuvenation have close relation to various dynamic relaxation modes which relate to the structural heterogeneity and flow defects. The mechanical relaxation

spectrum is used to reveal the relaxation mode, β relaxation process, which is crucial to the mechanical properties and is associated with cooperative atomic rearrangement (Ngai et al., 2013; Wang, 2011; Yu et al., 2018; Zhu et al., 2016).

The dynamic mechanical relaxation process is sensitive to the driving frequency. **Fig. 6** shows that the normalized loss modulus as a function of the temperature, and different driving frequencies (1-2-4-8 Hz) are applied with heating rate of 2 K/min (constant heating ramp test). The peak temperature of the β relaxation $T_{\beta p}$ shifts toward higher temperature by increasing the driving frequency. This tendency is consistent with the empirical equation of Arrhenius:

$$f = f_0 \exp(-E_\beta / k_B T) \quad (9)$$

where the f is driving frequency, E_β is the apparent activation energy of the β relaxation, k_B is Boltzmann constant, and f_0 is a characteristic frequency. We have reported that the correlation between E_β of the as-cast $La_{30}Ce_{30}Ni_{10}Al_{20}Co_{10}$ MG and T_g is in good agreement with the empirical relationship $E_\beta \approx (26 \pm 2)\, k_B T_g$ (Zhang et al., 2021). The results of DMA experiments performed on the La-based MG after mechanical cycling treatment are represented in **Figs. 7(a)-(c).** The data of the as-cast and pure aging samples are also included as references. It is obvious that these curves trace almost identical paths compared with that of the as-cast sample, indicating that their structures resemble each other. Note that an evident β relaxation process can be observed around 380 K from the normalized loss modulus in all states. The normalized loss modulus of the aged samples compared with a weaker β relaxation is significantly lower than that of the as-cast sample. Reviewed **Fig. 3**, the enhancement of mechanical cycling by increasing the mechanical cycling intensity is beneficial to inject more mechanical energy into the system and consequently the intensity of β relaxation increases while the peak temperature decreases, demonstrating a feature of structural rejuvenation. This is a surprising finding, since mechanical cycling can significantly rejuvenate MGs even at very few cycles (10^2 tension load cycles) and low frequencies (10^{-3} Hz). With relatively limited mechanical energy, there is a net structural relaxation indicated by the decrease of loss modulus and the suppression of β relaxation. Only when high enough

mechanical energy is applied, can the La-based MG translate into a rejuvenated state and present a larger loss modulus and stronger β relaxation. In the as-cast glass, the β relaxation peak is at 0.8~0.9T_g (Qiao et al., 2019; Wang, 2019). After severe plastic deformation (cold working), this is lowered to ~0.6 T_g (Méar et al., 2008). In addition, after thermal cycling between room temperature and liquid nitrogen temperature, this is at ~0.9T_g (Ketov et al., 2015). In our work, that is 0.85T_g for as-cast sample and 0.83~0.84T_g for the mechanical cycling treatment. There is quite a difference among the effect of mechanical cycling, thermal cycling, and cold working on the dynamic mechanical relaxation of MGs. Compared with thermal cycling developed by Ketov et al. (Ketov et al., 2015), mechanical cycling in this work is more effective to tailor the β relaxation and structural heterogeneity, and extending the range of the glassy state which has never achieved before.

It has been reported that the loss modulus or internal friction is associated with the atomic mobility of MGs (Wang et al., 2020; Wang et al., 2015; Yu and Samwer, 2014). The increase in loss modulus is an evident signal of enhanced atomic mobility, which indicates that the local atomic structure of deformed sample is modified effectively through mechanical cycling. Recent findings have revealed that the enhanced mobility of atoms is in favored regions around or within the shear bands after plastic deformation or in regions of higher internal stresses induced by thermal cycling (Hassanpour et al., 2021; Tian et al., 2017; Wang et al., 2021; Wang et al., 2022). The reason of occurrence of β relaxation in MGs can be understood by considering the heterogeneous structure at atomic scale, which includes alternative distribution of the closely packed and the loosely packed regions (Dmowski et al., 2010a; Kosiba et al., 2019; Zhu et al., 2016). It is reasonable to assume that the event of deformation unit formation occurs in the loosely packed regions where atoms can move easily in a local region. Local shear events are more likely to be activated in comparison to the closely packed regions. The observation that the β relaxation is easily enhanced by the mechanical cycling treatment indicates that the mobility of the underlying mobile species, i.e., the flow defects, can be created in the present alloy. Such a behavior means that more flow defects are

introduced into the MG matrix. Considering that the local atomic mobility in the β relaxation is correlated with enhanced structural heterogeneities, this result can be considered as strong evidence for the viscoelastic and the deformation mechanism associated with the β relaxation in MGs.

Considering T_g can only be changed within a few degrees, E_β should be nearly of a constant value for a given composition of MG. As the experimental results shown in **Figs. 7(d)-(f)**, E_β could be readily computed based on Eq. (9) and changes in a certain magnitude attributed to the distinct microstructural features. Specifically, compared with the as-cast MG ($E_\beta = 26.45\ k_B T_g$), E_β increases to 31.5 $k_B T_g$ (by 18.94%) after pure aging, 30.0 $k_B T_g$ (by 12.88%) for pure creep, respectively. However, the trend is reversed with decreasing from 26.98 to 19.83 $k_B T_g$ (mostly reduced by 25.02%) after mechanical cycling. During structural relaxation, the flow defect in glass decreases and, consequently, the activation energy for structural excitation tends to increase. If we roughly assume that the pure creep plays the same role in each sample, the maximum of rejuvenation efficiency during cyclic loading can be up to 44% in the range of applied stress. Clearly, the changes of E_β should be attributed to the mechanical cycling treatment, which affects the microstructure. The more the input mechanical energy, the lower the activation energy E_β for β relaxation. In one word, the reinforcement of the β relaxation validates the fact that more soft local regions are produced by mechanical cycling, which could promote atomic scale dynamics in MGs.

The activation energy and activation volume of the flow defect are usually regarded as the critical parameters in understanding the physical mechanism of the mechanical relaxation and plastic flow (Yang et al., 2016a; Yang et al., 2016b), and these two parameters can be detected by DMA. According to the cooperative shearing model (CSM) proposed by Johnson and Samwer, the relationship between the activation volume $V(T)$ and activation energy E_{csm} of deformation units can be described as (Johnson and Samwer, 2005):

$$V(T) = \frac{E_{csm}}{\frac{8}{\pi^2} G(T) \xi \gamma_c^2} \tag{10}$$

where $G(T)$ is the temperature dependent shear modulus, τ_c is a threshold shear resistance at absolutely zero temperature, $V(T)$ is flow defects volume, and constant strain $\gamma_c \approx 0.027$, and $\xi \approx 3$. Taken the Poisson ratio of La-based MG as ν≈0.32 (Wang, 2019) and $E_{csm} \approx E_{\beta}$, we can obtain the evolution of the shear modulus on temperature as:

$$G(T) = \frac{E(T)}{2(1+\nu)} = \frac{(E'(T)^2 + E''(T)^2)^{\frac{1}{2}}}{2(1+\nu)} \tag{11}$$

On the basis of Eqs. (10) and (11), the relation between the flow defects volume and temperature can be constructed and is depicted in **Figs. 8(a)-(d)**. It can be seen that V increases with temperature but decreases with the loading frequency (**Fig. 8(a)**), with a value from 4.0~5.0 nm^3, very close to the 5.5 nm^3 reported in $La_{60}Ni_{15}Al_{25}$ MG (Liu et al., 2012). Interestingly, the activation volume of flow defect continuously decreases with structural rejuvenation, as seen in **Figs. 8(b)-(d)**. In all cases, the aged sample possesses a maximum value while the mostly rejuvenated sample exhibits a minimum value. The above results can be understood by the following interpretation. As well known that the local atomic rearrangement in flow defect is corresponding to the characteristic relaxation time. The increase in loading frequency will shorten the characteristic relaxation time and suppress the structural relaxation process (i.e., frozen of flow defect), inducing a higher value of flow defect, which essentially lowers the viscosity (Li et al., 2014). On the other hand, the increase in loading frequency also reduces the free energy barrier relaxation in the deformed MG, leading to the acceleration of atomic diffusion in both the core and shell region, as formulated by (Spaepen, 1977):

$$D_{\mathrm{c}} = k_B T \lambda^2 / (6 V_{\mathrm{a}} \eta) \tag{12}$$

where D_{c} is the diffusion coefficient, λ is the jump distance, V_{a} is the volume of atom, and η is the viscosity. The increase in λ and decrease in η with increasing loading frequency will definitely enhance the diffusion coefficient. The strong diffusion capacity means that the aggregation of flow defects tends to be difficult. This is actually

what was observed in this work, as shown in **Fig. 8(a)**, i.e., the volume of flow units decreases with increasing loading frequency at a certain temperature. On the basis of the above analysis, it can be well understood that the decrease in V with increasing loading frequency in the deformed MG will result in a more homogeneous deformation spatiotemporally, which will promote material flow of MGs. In parallel, the improvement of atomic mobility in a rejuvenated MG also creates a difficulty in aggregation of flow defects.

Now the question is: How does mechanical cycling enhance the β relaxation? Based on the results obtained in the current work and for the sake of comparability we follow an idea by Perez [37], who proposed the concept of quasi-point defects (QPDs). Based on the heterogeneous structure, some nano-scale regions, so-called QPDs, correspond to the fluctuation of energy, density, enthalpy and entropy in the whole material. The atomic rearrangements activated by thermal and mechanical stimuli will preferentially take place in these defect sites. In the first stage of the deformation, QPDs are thermo-mechanically activated and oriented along the maximum shear stress plane. The directed activation of QPDs is associated with the β relaxation process. Referring to Arrhenius response, the characteristic time τ to overcome the energy barrier can be described by rewriting Eq. (9) as:

$$\tau = \tau_{\mathrm{a}} \exp(E_{\beta} / k_{\mathrm{B}} T) \tag{13}$$

where τ_{a} is the pre-exponential time. This process is associated with the non-elastic strain component γ_{β} at the macroscopic scale. The corresponding strain rate $\dot{\gamma}_{\beta}$ decays linearly to the equilibrium state γ_{β}^{∞} with the characteristic time τ:

$$\dot{\gamma}_{\beta} = \frac{\gamma_{\beta}^{\infty} - \gamma_{\beta}}{\tau_{\beta}} \tag{14}$$

γ_{β}^{∞} can be defined by a limited strain value, which depends on the change of compliance ΔJ_{β} induced by β relaxation and the activation stress σ_{α}:

$$\begin{cases} \gamma_{\beta}^{\infty} = \sigma_{\alpha}\Delta J_{\beta} \\ \Delta J_{\beta} = J_{\beta\_r} - J_{\beta\_u} = \dfrac{1}{E_{\beta\_r}} - \dfrac{1}{E_{\beta\_u}} \end{cases} \tag{15}$$

where the elastic modulus E is the reciprocal of the compliance J, the subscripts 'β_u' and 'β_r' is the unrelaxed and relaxed states, i.e., the beginning and ending the β relaxation process. A distribution function of activation energy is used to describe the heterogenous defect sites, and this is naturally equivalent to a distribution of the relaxation times. A discrete normalized Gumbel distribution was chosen from the thermodynamic considerations:

$$w_i = \frac{\exp\left\{B\ln\left(\frac{\tau_{\mathrm{i}}}{\bar{\tau}}\right) - \exp\left[B\ln(\frac{\tau_{\mathrm{i}}}{\bar{\tau}})\right]\right\}}{\sum_{\mathrm{i}}\exp\left\{B\ln\left(\frac{\tau_{\mathrm{i}}}{\bar{\tau}}\right) - \exp\left[B\ln(\frac{\tau_{\mathrm{i}}}{\bar{\tau}})\right]\right\}} \tag{16}$$

where the distribution parameter B is in the range of 0 to 1, τ_{i} is the characteristic time of the i-th unit, $\bar{\tau}$ is the mean characteristic time and w_{i} is the corresponding probability weight. The macroscopic strain rate related to the β relaxation corresponds to the sum of all distributed processes. Thus, each isolated relaxation unit and its corresponding kinetic equation contributes to a fraction of the intensity of the total process. Thus, the single characteristic time in Eq. 13 can be replaced by the discrete normalized Gumbel distribution of time $\tau_{\beta}^{\mathrm{i}}$ and then Eq. 14 is reformulated:

$$\dot{\gamma}_{\beta} = \sum_{\mathrm{i}=1}^{\mathrm{n}} \frac{(w_{\mathrm{i}}\sigma_{\alpha}\Delta J_{\beta}) - \gamma_{\beta}^{\mathrm{i}}}{\tau_{\beta}^{\mathrm{i}}} \tag{17}$$

The sheared micro-domains nucleate by QPDs and progressively develop in the maximum shear plane at a constant stress. Furthermore, new sheared micro-domains nucleate by the activation of QPDs. To some extent, the concept of QPDs is similar to other terminologies as that used in the literature, e.g., shear transition zones (STZs) or CSM mentioned above.

The elastic energy stored drives the sheared micro-domains shrink when the applied stress is removed. The reversible strain γ_{an} with sufficient time is corresponding to the anelastic component at the macroscopic scale. Besides, the percolation of expanding

sheared micro-domains is corresponding to irreversible deformation γ_{vp} (the visco-plastic component). The rearrangements responsible for the visco-plastic deformation (related to the α relaxation) are more complex than that of the anelastic deformation (associated with the β relaxation). In fact, there are hierarchical correlation among the mechanical relaxations, i.e., they involve more and more relaxation units and require longer and longer time to be completed. The time scale needed for these movements varies beginning from the time for the completed elementary movement to the time for annihilation of the sheared micro-domains. The latter is defined as:

$$\tau_{mol} = \tau_0 \left(\frac{\tau_{\beta\_i}}{\tau_0}\right)^{\frac{1}{\chi}} \tag{18}$$

where τ_0 is a pre-parameter, τ_{β_i} is the characteristic time of the ith elementary deformation unit, χ is a correlation factor which is related to the concentration of defects. For example, $\chi = 0$ for the fully ordered lattice structure, corresponding to an ideal crystal. In this case, the movement of a structural unit depends on all other units via interatomic interactions. In the opposite case, $\chi = 1$ stands for the fully disordered structure, corresponding to the ideal gas. The motion of a structural unit is fully independent of others, i.e., there is no enthalpic interaction and entropy dominates thermodynamics. These elementary deformation units can be regarded as the movements involved in the β relaxation. The intensity of the movements shows an apparent dependence on the heterogeneity degree, i.e., the density of defects. The distribution of the characteristic times for the anelastic process around a mean value:

$$\tau_{an} = \tau_{mol}\chi^{\frac{1}{\chi}} \tag{19}$$

following the Gumbel distribution with a width equal to χ. As for the β relaxation, the macroscopic strain rate can be described as a sum of local shearing characterized by the distribution of characteristic times:

$$\dot{\gamma}_{an} = \sum_{i=1}^{n} \frac{(w_{an}^{i}\gamma_{an}^{\infty}) - \gamma_{an}^{i}}{\tau_{an}^{i}} \tag{20}$$

where $w_{\mathrm{an}}^{\mathrm{i}}$ are the relative weights of the times $\tau_{\mathrm{an}}^{\mathrm{i}}$, $\gamma_{\mathrm{an}}^{\infty}$ is the equilibrium strain for the anelastic process and can be calculated by the β relaxation as:

$$\gamma_{\mathrm{an}}^{\infty} = \sigma_{\alpha} \Delta J_{\mathrm{an}} \tag{21}$$

where ΔJ_{an} is the change of the compliance correlated to the anelastic process. As we mentioned above, χ is related to the heterogeneity degree, and then it is connected to the evolution of microstructure. The MGs remain in a frozen or iso-configurational state below T_{g} without aging and rejuvenation and, thus, χ remains constant. When the temperature is above T_{g}, the system shifts to a metastable thermodynamic equilibrium state, and χ increases linearly with temperature. Finally, the following temporal evolution law for the correlation parameter χ are added:

$$\begin{cases} \chi(T) = \chi(T_{\mathrm{g}}) \\ \chi(T) = \chi(T_{\mathrm{g}}) + \chi_0 (T - T_{\mathrm{g}}) \end{cases} \tag{22}$$

where χ_0 depends on the specific material. Therefore, Eqs. (13)-(22) can be explicitly integrated. Then, the addition of all these processes successively involved leads to the expression of the general compliance:

$$J(t) = J_{\mathrm{el}} + \Delta J_{\beta} \sum_{\mathrm{i}=1}^{\mathrm{n}} w_{\beta}^{\mathrm{i}} \left[1 - \exp\left(\frac{-t}{\tau_{\beta}^{\mathrm{i}}} \right) \right] \tag{23}$$

where J_{el} is the elastic compliance, taken as the inverse of the unrelaxed elastic modulus E_{β_u}. The contributions of relaxations faster than the β relaxation are assimilated to the instantaneous response. Laplace transform of Eq. 23 directly shows the expression of the frequency-dependent compliance $J^*(\omega)$ of MGs:

$$J^*(\omega) = J_{\mathrm{el}} + J_{\beta} \sum_{\mathrm{i}=1}^{\mathrm{n}} \frac{w_{\beta}^{\mathrm{i}}}{1 + \mathrm{i}\omega\tau_{\beta}^{\mathrm{i}}} = J'(\omega) + \mathrm{i}J''(\omega) \tag{24}$$

where ω is the angular frequency (equal to $2\pi f$). The real part of $J'(\omega)$ and the imaginary part $J''(\omega)$ are storage compliance and loss compliance, respectively. Both storage and loss modulus (respectively, E' and E'') can be simply deduced from $J'(\omega)$

and $J''(\omega)$.

Among them, there are five parameters devoted to the characterization of the β relaxation. The unrelaxed and relaxed modulus (E_{β_u} an E_{β_r}) are directly read on the E' versus temperature curve. The β relaxation activation energy E_{β} is directly obtained by the multiple frequency test fitting. The distribution parameter B reached from the fit of the E'' versus temperature curve in the β relaxation domain. Based on the QPD model, the evolution of E''/E_{u} on temperature suffering different mechanical cycling can be simulated by Eq. (24), as shown in **Fig. 9(a)**. Mathematically, the distribution parameter B reflects the distribution width of samples. A higher value of B corresponds to a more heterogenous and wider distribution. Here, B determines the distribution of the relaxation units and is therefore intimately correlated to the microscopic configuration of MGs. The values of B is 0.24, 0.26, and 0.30 for rejuvenation (25-175 MPa), as-cast and aging states, respectively, which show fairly compatible changes in MG ribbons. In a common perspective, the decrease of B with the rejuvenation of MG structure implies an enhancement of structural heterogeneity. By proper fitting, the distribution of flow defects is extracted and plotted in **Figs. 9(b)** and **(c)** as functions of temperature and characteristic relaxation time. Compared to the as-cast sample, the characteristic relaxation time reduces significantly after mechanical cycling but increases after physical aging. A similar phenomenon is also observed in the evolution with temperature. These indicate that mechanical cycling results in the activation of more flow defects with different relaxation times, contributing to the macroscopic relaxation process. The wider relaxation time distribution with structural rejuvenation implies that more types of flow defects are activated. The faster modes can be attributed to the shortening of the relaxation time of each flow defect with a specific activation temperature.

MGs have been depicted to contain flow defects, identified from structure information(Cao et al., 2019). These soft regions or geometrically disfavored motifs from atomic packing are susceptible to rearrangement under mechanical deformation (Ma, 2015). The population of activated flow defects in mechanical cycling, which

depends on stress rate, stress amplitude, and mean stress, is responsible for the homogeneous flow. The coupling of thermal activation and stress leads to excitation of a majority of flow defects via collective rearrangements, and if they are percolated through the system, flow in a homogeneous manner would then ensue (Cao et al., 2019; Şopu et al., 2020). The increase of the mechanical cycling intensity activates defects with shorter relaxation time in "core" and "shell" regions. These defects collapse the "shell" region and finally retained in the system because of lack of sufficient time for internal stress relaxation (Galindo-Torres et al., 2018). At the same time, the transition from "shell" to "core" regions drives MGs towards higher energetic state, which broadens the distribution of density and characterizes time of β relaxation units.

3.3 Visualizing structural evolution

As usual, the mechanical properties of a glass depend on the structural relaxation and consequently on the rejuvenation. In order to describe the structure state, it is crucial to find an indicator capable of depicting the physical situation. The concept of fictive temperature T_f is in principle an elegant way of quantifying the degree of disorder and such that the physical properties (Ketkaew et al., 2018). The fictive temperature at which the frozen-in liquid structure is at equilibrium has been widely used to characterize the mechanical/physical properties of MGs such as the plasticity (Kumar et al., 2013; Magagnosc et al., 2014). Physical aging results in structural relaxation and a reduction in T_f (Luckabauer et al., 2019). It is reasonable to speculate that the mechanical cycling either preserves or even increases T_f in our alloy (**Fig. 10(a)**). It is well-known that mechanical deformation converts mechanical energy into thermal energy and raises the effective temperature, for example, in shear bands (Fornell et al., 2009; Jiang et al., 2008; Wu et al., 2011). In other words, atomic displacements out of the atomic cage due to deformation increase the randomness of the structure. For mechanical cycling, apparently mechanical energy translates into an increase in the internal energy cancelling the effect of structural relaxation. The balance between the effects of structural relaxation and structural rejuvenation due to deformation depends on various factors, such as stress amplitude, stress rate, and mean stress. From the above

results, a diagram of the competition between the rejuvenation and aging of a MG can be constructed, which is Moreover, the threshold value of mechanical cycling intensity between rejuvenation and structural relaxation can be used to broadly modulate the structural heterogeneity of MGs. illustrated in **Fig. 10(b)**.

A schematic explanation of the relationship between aging, rejuvenation and β relaxation in MGs is shown in the inset of **Fig. 10(a)** from a microstructural perspective. Both the rejuvenation and β relaxation occur in isolated and loosely packed flow defects in MG. The rejuvenation activates the potential flow defects, and the density of the liquid-like flow defects then increases. Therefore, the intensity of the β relaxation peak originating from the flow defects will then increase and shift to low activation energy side after rejuvenation while decrease and shift to high activation energy side after aging.

To understand the change of the structural state of MGs from a general perspective, we adopt the potential energy landscape (PEL) concept (Debenedetti and Stillinger, 2001), which has been widely applied to investigate plastic deformation (Harmon et al., 2007), physical aging (Lüttich et al., 2018), and rejuvenation (Sun et al., 2016) of MGs. The change of the β relaxation process can be explained from the viewpoint of PEL and different stability of the system. Here, we would like to underline that the change of the β relaxation process is attributed to the change of distance (in configurational space) and density of sub-basins. For these reasons, an obvious change in the distribution of relaxation units is observed. The mechanical cycling drives the system to a more unstable state with smaller average distances between sub-basins; consequently, the activation energy barrier of β relaxation process decreases and the β relaxation appears as a more independent peak. Alternatively, the average separation between sub-basins is larger in a more stable system. Such configuration is of a lower degree of heterogeneity, which leads to an increased activation energy.

The rejuvenation in MGs is the process that a system escapes from one deep local minimum to another one at a higher energy state, which corresponds to an activation hopping between neighboring inherent states after surmounting energy barrier. The activation of the frozen flow defects accommodating the plastic deformation is confined

within the elastic matrix. This is corresponding to a stress-induced rejuvenation. The mechanically stress-induced rejuvenation, equivalent to the thermally activated rejuvenation, can significantly enhance the atomic mobility or decrease the viscosity by inducing a glass-to-supercooled liquid transition. Consequently, the rejuvenation associated with the collapse of the elastic matrix could be regarded as the locally α relaxation. Both the rejuvenation and β relaxation in MGs can be treated as a flow phenomenon which is excitated by thermal fluctuation or mechanical work. The rejuvenation raises the potential energy of a MG through activation of the flow defects. As we have mentioned above, it is recognized that the activation energy of β relaxation is the same as that for the operation of flow defects and for the ductile-to-brittle transition (Ngai and Capaccioli, 2004; Yu et al., 2010). The rejuvenation raises the energy of a MG through successive activation of β relaxation. Therefore, the rejuvenation in MGs can be regarded as the percolation of a series of β relaxation in nano-scale regions. Experimental evidence shows that MG with a pronounced β relaxation shows enhanced ductility (Yu et al., 2014; Yu et al., 2013). On the other hand, the rejuvenation can also make a MG ductile (Ketov et al., 2015). This is another implication of the link between rejuvenation and β relaxation.

The correlation and difference among the various structural indicators of the aged and rejuvenated MG is briefly summarized here. The effective structural parameters which give a consistent description of the structural state of a MG is indeed required. For example, local regions in a rejuvenated MG should have higher potential energy, higher fictive temperature, and they should contain more flow defects. In **Fig. 10(c)**, we illustrate the correlation between these parameters, as well as the structural state they correspond to. The striking contrast between aged and rejuvenated MGs may be an excellent ridge that can be adopted to tailor the structure and properties of MGs, owing to the fact that it conveys more dynamic information, and it is general and system independent. Moreover, it helps to construct a physics motivated constitutive model, among which the flow defect, potential energy, or fictive temperature should be a priority.

4. Conclusions

Mechanical cycling even at very few cycles (10^2 tension load cycles) and low frequencies (10^{-3} Hz) can adjust the structure locally and modulate the degree of structural heterogeneity of MGs. Depending on the thermodynamic or mechanical conditions, MGs can be either structurally relaxed or rejuvenated to a remarkable extent. This way bears great potential for producing highly metastable MGs and thus extending the range of the glassy state without introducing extrinsic defects like shear bands. The increase of the mechanical cycling intensity (i.e., stress amplitude, stress rate or mean stress) injects more mechanical energy into MGs. This additional mechanical energy, which suppresses or surpasses aging, is responsible for the rejuvenation. Consequently, our method can be applied to a broad modulation of structural heterogeneity. The two-phases model shows that amounts of frozen flow defects are woken when a dynamic cyclic loading is applied on MGs.

Dynamic mechanical analyzer illustrates that the evolution of the β relaxation suffers from mechanical cycling. With the present approach, one can obtain highly metastable and structurally heterogeneous state in MGs, which enables us to assess the nature of the correlation among flow defect, rejuvenation and the β relaxation. Activation energy of the β relaxation decreases from 0.92 eV to almost 0.82 eV. The intensity of β relaxation is increased and shifts to lower activation energy side upon rejuvenation. In addition, the rejuvenation also expands the distribution of the relaxation units while aging plays an opposite role.

Acknowledgements

This work is supported by the NSFC (Grant No. 51971178), the Natural Science Basic Research Plan for Distinguished Young Scholars in Shaanxi Province (Grant No. 2021JC-12) and the Natural Science Foundation of Chongqing (Grant No. cstc2020jcyj-jqX0001). The investigation of L.T. Zhang is sponsored by Innovation Foundation for Doctor Dissertation of Northwestern Polytechnical University (Grant No. CX2021015). YJW was financially supported by NSFC (Grant No. 12072344) and the Youth Innovation Promotion Association of the Chinese Academy of Sciences. YY

acknowledges financial support from Research Grant Council (RGC), the Hong Kong government through the General Research Fund (GRF) with the grant numbers CityU11200719 and CityU11213118.

Captions of the Figures and Tables

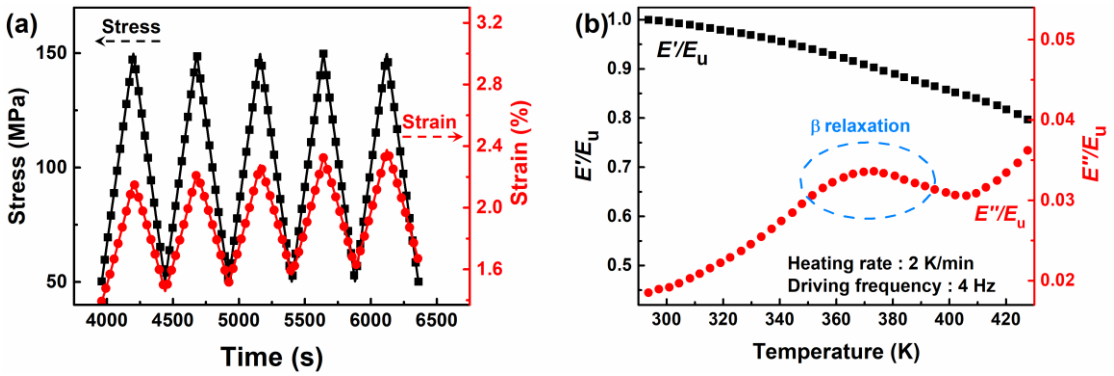

Fig. 1 (a) Stress-strain curves of La-based MG from a subset of 120 tensile loading/unloading cycles in the linear elastic regime. (b) Dynamic relaxation spectrum as a function of temperature. Conspicuous β relaxation feature is noticed by a peak in loss modulus at approximately 370 K.

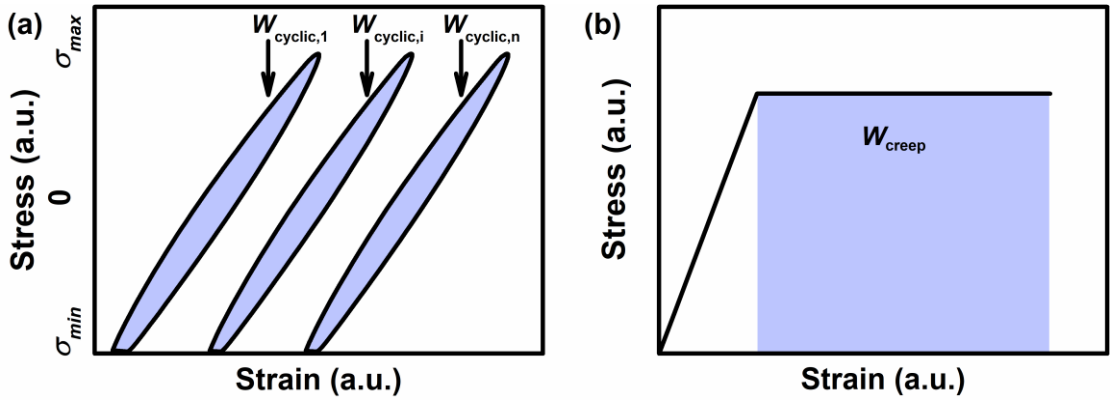

Fig. 2 Schematic representation of the hysteresis loops during pure cyclic loading in (a), and creep in (b). The dash area is corresponding to the mechanical work W_{cyclic} and W_{creep}, respectively.

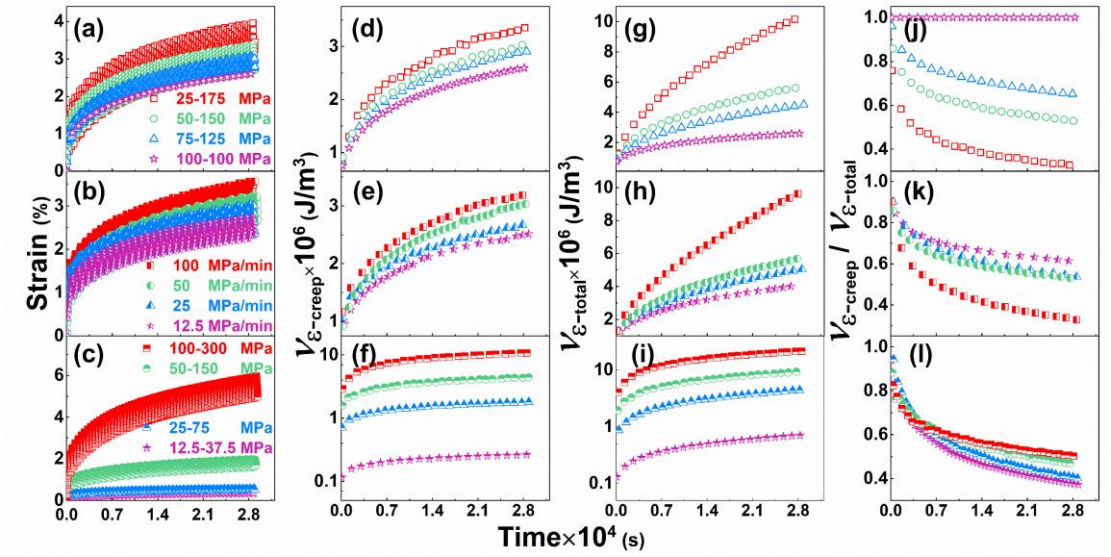

753

754 Fig. 3 Creep of of $La_{30}Ce_{30}Ni_{10}Al_{20}Co_{10}$ MG. Time dependence of (a-c) strain, (d-f)

755 ν_{ε_creep}, (g-i) ν_{ε_total}, (j-l) $\nu_{\varepsilon\_creep}/\nu_{\varepsilon\_total}$ at different stress amplitude, stress rate, and

756 mean stress, respectively.

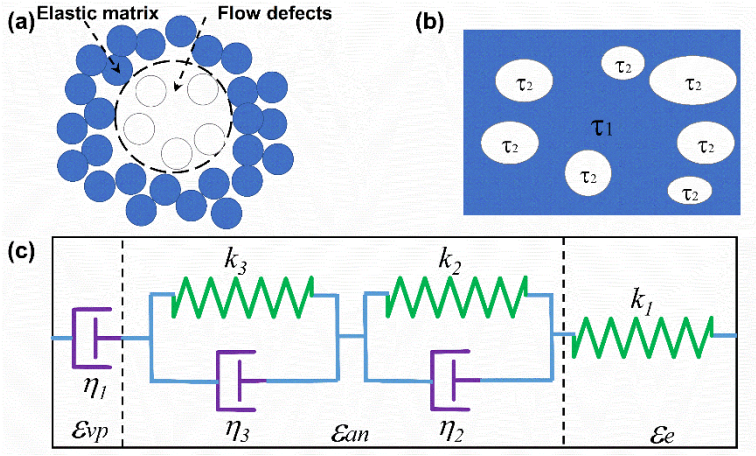

Fig. 4 Maxwell-Voigt model with dynamically heterogenous flow defects. (a) The schematic illustration of MG structure composed of elastic matrix and flow defects. (b) The spatial distribution of the versatile relaxation processes with different characteristic relaxation times; (c) The Maxwell-Voigt model used for analyzing creep deformation.

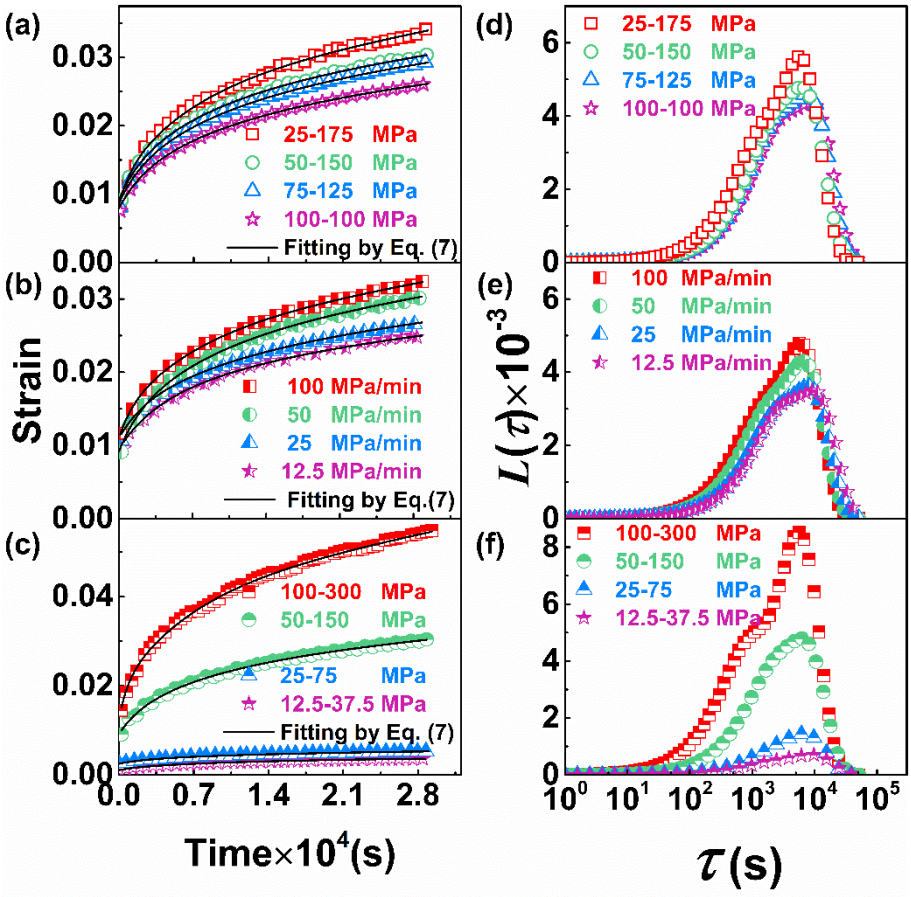

762

763 Fig. 5 Strain versus time at different (a) stress amplitude, (b) stress rate, and (c) mean
764 stress, respectively. Solid lines are the best fits by Eq. (1); (d)—(f) Corresponding
765 spectra of relaxation times based on the anelastic part of creep curves.

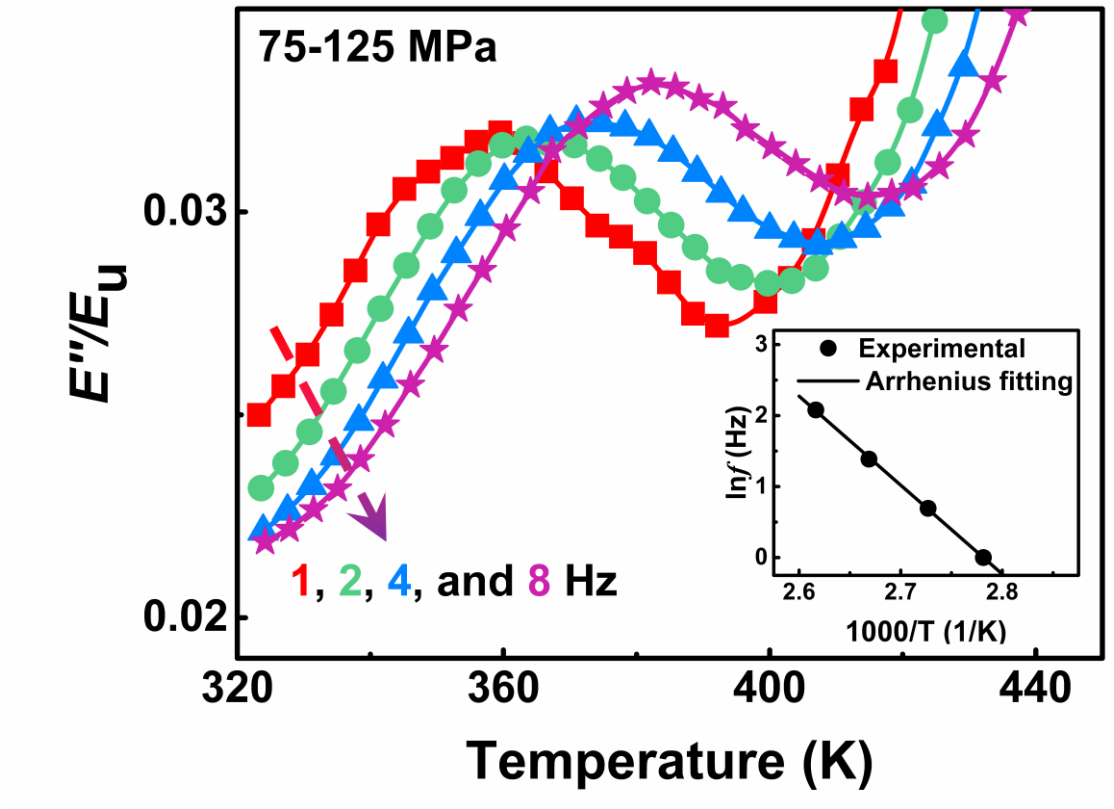

Fig. 6 Evolution of normalized loss modulus E''/E_u as a function of temperature at different driving frequencies (1, 2, 4 and 8 Hz, respectively). Solid lines are the best fits by Eq. (1). The inset is an Arrhenius plot of frequency versus temperature.

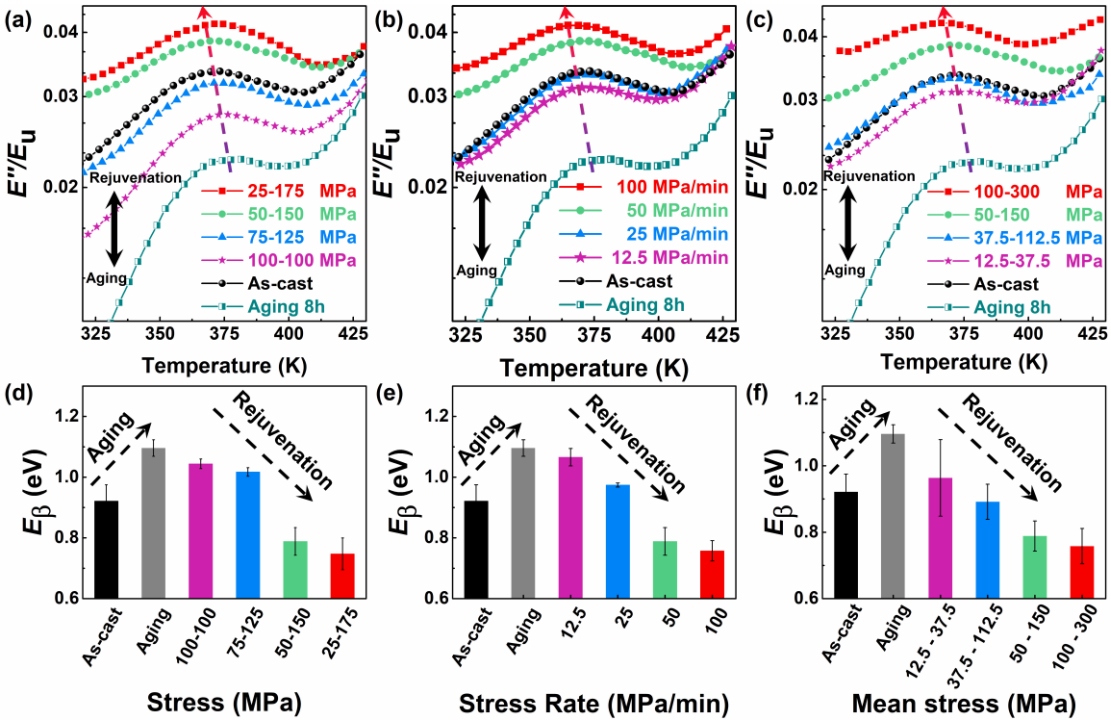

771

772 Fig. 7 Rejuvenation of $La_{30}Ce_{30}Ni_{10}Al_{20}Co_{10}$ MG. Evolution of normalized loss
773 modulus E''/E_u on temperature at different (a) stress amplitude, (b) stress rate, and (c)
774 mean stress, respectively. The driving frequency is 4 Hz and heating rate is 2 K/min.
775 The as-cast and aged samples are added as references; (d)—(f) Variation of activation
776 energy of β relaxation corresponding to (a)—(c).

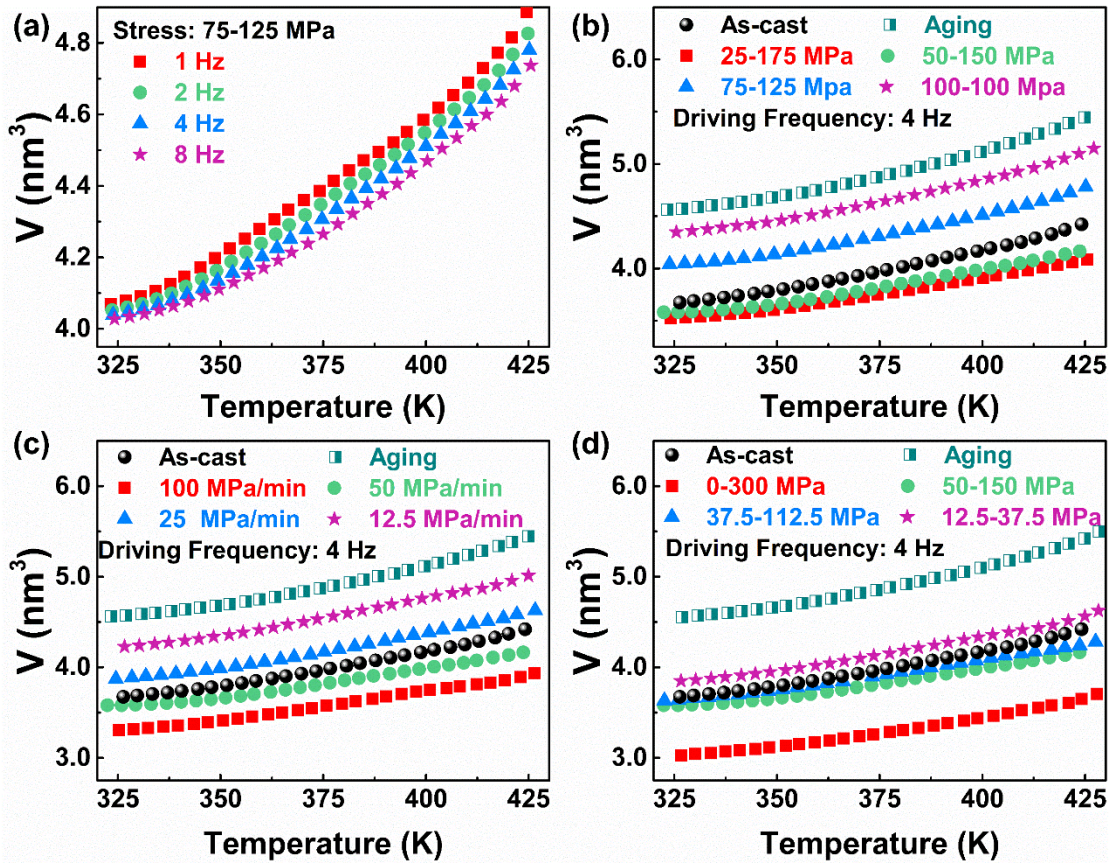

Fig. 8 Temperature-dependent activation volume V at different conditions of (a) driving frequencies, (b) stress amplitude, (c) stress rate and (d) mean stress, respectively.

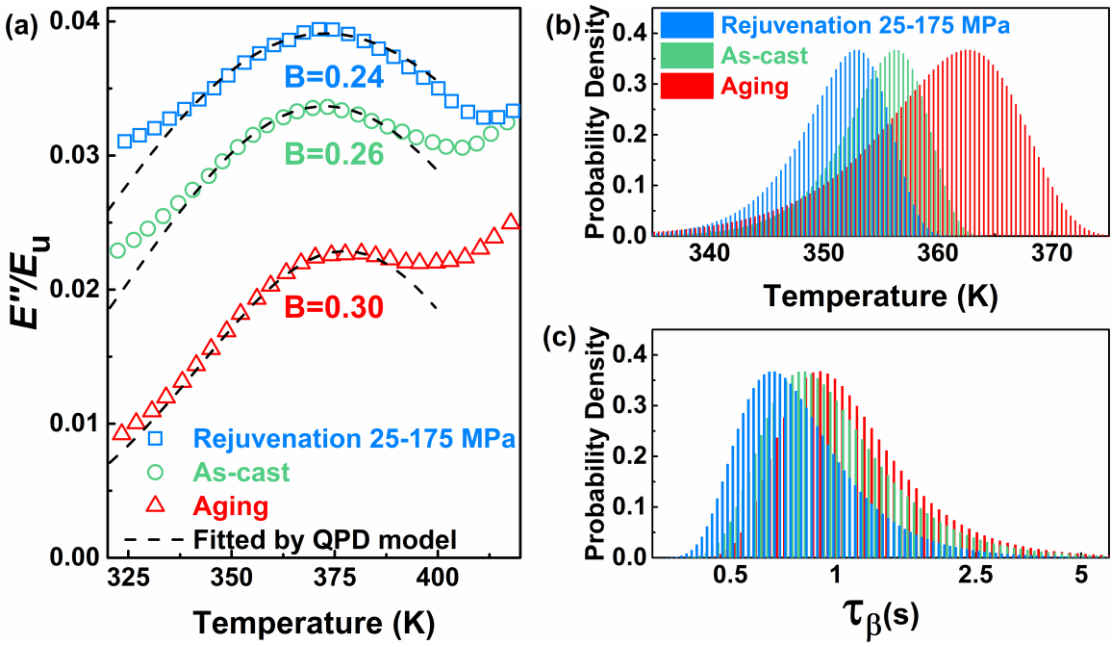

Fig. 9 Temperature dependence of the normalized loss modulus E''/E_u for the rejuvenated, as-cast and aging state of $La_{30}Ce_{30}Ni_{10}Al_{20}Co_{10}$ MG. The dash lines denote fits by QPD model, Intensity of β relaxation versus (b) temperature, and (c) relaxation time for the rejuvenated, as-cast, and aging state of glass, respectively.

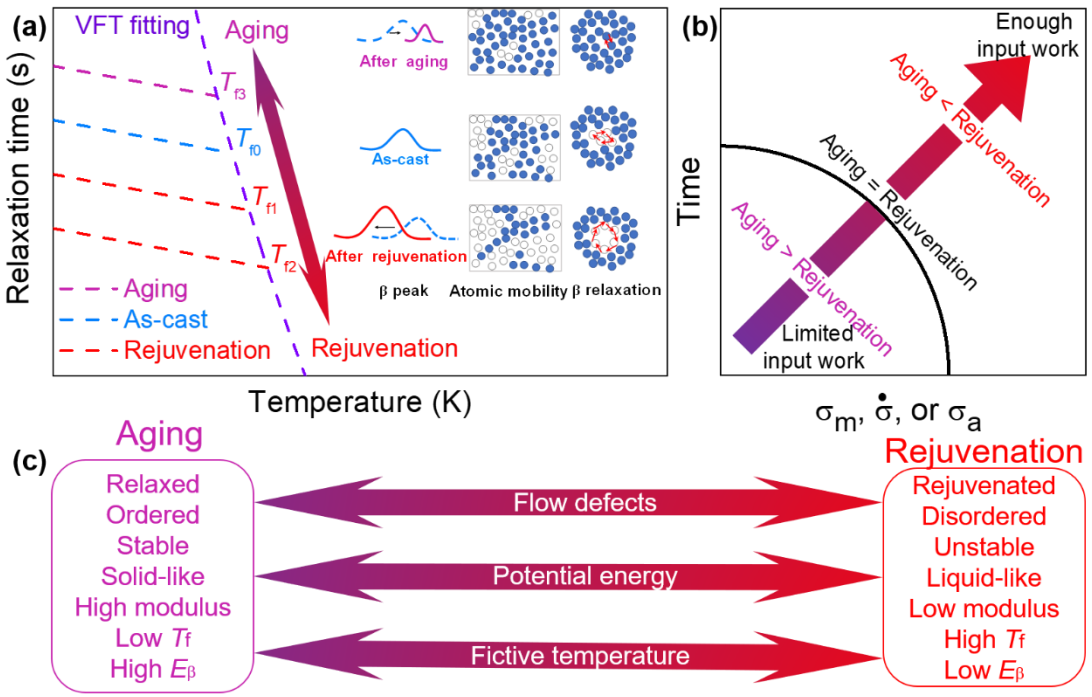

Fig. 10 Rejuvenation diagram. (a) Schematic illustration of the effect of aging and rejuvenation on the evolution of the relaxation time. The inset shows the correlation between flow defect, aging, rejuvenation and β relaxation process from a microscopic perspective; (b) Aging and rejuvenation map in cyclic loading; (c) Structural indicators of aged and rejuvenated MGs and their general relationship. The keywords used to qualitatively describe the structural states correspond to the high and low ends in the spectrum of each of these indicators.

Table 1 The fitting parameters for creep of La-based MG using the Maxwell-Voigt model.

	Stress [MPa]	ε_1 $\times 10^{-2}$	τ_1 [s]	$\varepsilon_2 \times 10^{-2}$	τ_2 [s]	ε_{vp} $\times 10^{-7}$ [s^{-1}]	$\varepsilon_2/\varepsilon_1$
Stress amplitude [MPa]	100-100	0.44±0.04	2341.65±12.08	1.02±0.05	11421.16±132.48	1.54±0.20	2.32
	75-125	0.43±0.03	2113.23±87.35	1.08±0.02	9987.10±658.45	1.98±0.12	2.51
	50-150	0.38±0.06	1801.65±216.90	1.12±0.03	8283.15±1018.91	2.28±0.22	2.95
	25-175	0.37±0.05	1107.52±215.20	1.34±0.04	7112.00±684.00	2.94±0.22	3.62
Stress rate [MPa/min]	12.5	0.36±0.03	2544.09±298.36	0.82±0.03	12711.05±485.00	1.46±0.08	2.28
	25	0.32±0.01	2011.31±599.34	0.85±0.01	10169.00±1001.77	1.60±0.32	2.66
	50	0.38±0.06	1801.65±216.90	1.12±0.03	8283.15±1018.91	2.28±0.22	2.95
	100	0.31±0.04	1169.86±180.19	1.14±0.03	7381.59±761.11	2.44±0.21	3.68
Mean stress [MPa]	25	0.06±0.001	1843.00±186.84	0.17±0.01	10886.54±1598.23	0.18±0.04	2.93
	50	0.08±0.01	1826.58±278.42	0.24±0.01	8599.14±1741.07	0.29±0.04	3.00
	100	0.38±0.06	1801.65±216.90	1.12±0.03	8283.15±1018.91	2.28±0.22	2.95
	200	0.70±0.08	757.58±181.56	2.13±0.08	6835.17±708.56	4.80±0.41	3.04

Reference

Argon, A.S., 1979. Plastic deformation in metallic glasses. Acta Metall. 27, 47-58.

Ashby, M.F., Greer, A.L., 2006. Metallic glasses as structural materials. Scr. Mater. 54, 321-326.

Barriere, T., Gabrion, X., Holopainen, S., Jokinen, J., 2020. Testing and analysis of solid polymers under large monotonic and long-term cyclic deformation. Int. J. Plast. 135,

102781.

Cao, P., Short Michael, P., Yip, S., 2019. Potential energy landscape activations governing plastic flows in glass rheology. Proc. Natl. Acad. Sci. 116, 18790-18797.

Casalini, R., Roland, C.M., 2009. Aging of the Secondary Relaxation to Probe Structural Relaxation in the Glassy State. Phys. Rev. Lett. 102, 035701.

Castellero, A., Moser, B., Uhlenhaut, D.I., Torre, F.H.D., Löffler, J.F., 2008. Room-temperature creep and structural relaxation of Mg–Cu–Y metallic glasses. Acta Mater 56, 3777-3785.

Chen, Y., Dai, L.H., 2016. Nature of crack-tip plastic zone in metallic glasses. Int. J. Plast. 77, 54-74.

Chen, Y., Jiang, M.Q., Dai, L.H., 2013. Collective evolution dynamics of multiple shear bands in bulk metallic glasses. Int. J. Plast. 50, 18-36.

Concustell, A., Sort, J., Greer, A., Baró, M., 2006. Anelastic deformation of a $Pd_{40}Cu_{30}Ni_{10}P_{20}$ bulk metallic glass during nanoindentation. Appl. Phys. Lett. 88, 171911.

Debenedetti, P.G., Stillinger, F.H., 2001. Supercooled liquids and the glass transition. Nature 410, 259-267.

Ding, G., Li, C., Zaccone, A., Wang, W.H., Lei, H.C., Jiang, F., Ling, Z., Jiang, M.Q., 2019. Ultrafast extreme rejuvenation of metallic glasses by shock compression. Sci. Adv. 5, eaaw6249.

Dmowski, W., Iwashita, T., Chuang, C.P., Aimer, J., Egami, T., 2010a. Elastic Heterogeneity in Metallic Glasses. Phys. Rev. Lett. 105, 205502.

Dmowski, W., Iwashita, T., Chuang, C.P., Almer, J., Egami, T., 2010b. Elastic Heterogeneity in Metallic Glasses. Phys. Rev. Lett. 105, 205502.

Evenson, Z., Naleway, S., Wei, S., Gross, O., Kruzic, J., Gallino, I., Possart, W., Stommel, M., Busch, R., 2014. β relaxation and low-temperature aging in a Au-based bulk metallic glass: From elastic properties to atomic-scale structure. Phys. Rev. B 89, 174204.

Fiocco, D., Foffi, G., Sastry, S., 2013. Oscillatory athermal quasistatic deformation of

a model glass. Phys. Rev. E 88, 020301.

Fiocco, D., Foffi, G., Sastry, S., 2014. Encoding of Memory in Sheared Amorphous Solids. Phys. Rev. Lett. 112, 025702.

Fornell, J., Concustell, A., Suriñach, S., Li, W.H., Cuadrado, N., Gebert, A., Baró, M.D., Sort, J., 2009. Yielding and intrinsic plasticity of Ti–Zr–Ni–Cu–Be bulk metallic glass. Int. J. Plast. 25, 1540-1559.

Galindo-Torres, S.A., Zhang, X., Krabbenhoft, K., 2018. Micromechanics of Liquefaction in Granular Materials. Phys. Rev. Appl. 10, 064017.

Greer, A.L., Cheng, Y.Q., Ma, E., 2013. Shear bands in metallic glasses. Mater. Sci. Eng., R 74, 71-132.

Greer, A.L., Sun, Y.H., 2016. Stored energy in metallic glasses due to strains within the elastic limit. Philos. Mag. 96, 1643-1663.

Guan, P., Chen, M., Egami, T., 2010. Stress-Temperature Scaling for Steady-State Flow in Metallic Glasses. Phys. Rev. Lett. 104.

Harmon, J.S., Demetriou, M.D., Johnson, W.L., Samwer, K., 2007. Anelastic to Plastic Transition in Metallic Glass-Forming Liquids. Phys. Rev. Lett. 99, 135502.

Hasanpour, K., Ziaei-Rad, S., Mahzoon, M., 2009. A large deformation framework for compressible viscoelastic materials: Constitutive equations and finite element implementation. Int. J. Plast. 25, 1154-1176.

Hassanpour, A., Vaidya, M., Divinski, S.V., Wilde, G., 2021. Impact of cryogenic cycling on tracer diffusion in plastically deformed Pd40 Ni40 P20 bulk metallic glass. Acta Mater 209, 116785.

Jiang, W.H., Fan, G.J., Liu, F.X., Wang, G.Y., Choo, H., Liaw, P.K., 2008. Spatiotemporally inhomogeneous plastic flow of a bulk-metallic glass. Int. J. Plast. 24, 1-16.

Johari, G.P., 2002. Localized molecular motions of β-relaxation and its energy landscape. J. Non·Cryst. Solids 307-310, 317-325.

Johari, G.P., Goldstein, M., 1970. Viscous liquids and the glass transition. II. Secondary relaxations in glasses of rigid molecules. J. Chem. Phys. 53, 2372-2388.

Johnson, W., Samwer, K., 2005. A universal criterion for plastic yielding of metallic glasses with a $(T/T_g)^{2/3}$ temperature dependence. Phys. Rev. Lett. 95, 195501.

Johnson, W.L., 1986. Thermodynamic and kinetic aspects of the crystal to glass transformation in metallic materials. Prog. Mater. Sci. 30, 81-134.

Ketkaew, J., Chen, W., Wang, H., Datye, A., Fan, M., Pereira, G., Schwarz, U.D., Liu, Z., Yamada, R., Dmowski, W., Shattuck, M.D., O'Hern, C.S., Egami, T., Bouchbinder, E., Schroers, J., 2018. Mechanical glass transition revealed by the fracture toughness of metallic glasses. Nat. Commun. 9, 3271.

Ketov, S.V., Sun, Y.H., Nachum, S., Lu, Z., Checchi, A., Beraldin, A.R., Bai, H.Y., Wang, W.H., Louzguine-Luzgin, D.V., Carpenter, M.A., Greer, A.L., 2015. Rejuvenation of metallic glasses by non-affine thermal strain. Nature 524, 200-203.

Khan, A., Zhang, H., 2001. Finite deformation of a polymer: experiments and modeling. Int. J. Plast. 17, 1167-1188.

Khan, A.S., Lopez-Pamies, O., 2002. Time and temperature dependent response and relaxation of a soft polymer. Int. J. Plast. 18, 1359-1372.

Khan, A.S., Lopez-Pamies, O., Kazmi, R., 2006. Thermo-mechanical large deformation response and constitutive modeling of viscoelastic polymers over a wide range of strain rates and temperatures. Int. J. Plast. 22, 581-601.

Kosiba, K., Şopu, D., Scudino, S., Zhang, L., Bednarcik, J., Pauly, S., 2019. Modulating heterogeneity and plasticity in bulk metallic glasses: Role of interfaces on shear banding. Int. J. Plast. 119, 156-170.

Küchemann, S., Maaß, R., 2017. Gamma relaxation in bulk metallic glasses. Scr. Mater. 137, 5-8.

Kumar, G., Neibecker, P., Liu, Y.H., Schroers, J., 2013. Critical fictive temperature for plasticity in metallic glasses. Nat. Commun. 4, 1536.

Lacks, D.J., Osborne, M.J., 2004. Energy Landscape Picture of Overaging and Rejuvenation in a Sheared Glass. Phys. Rev. Lett. 93, 255501.

Li, N., Xu, X., Zheng, Z., Liu, L., 2014. Enhanced formability of a Zr-based bulk metallic glass in a supercooled liquid state by vibrational loading. Acta Mater 65, 400-

411.

Liu, S.T., Wang, Z., Peng, H.L., Yu, H.B., Wang, W.H., 2012. The activation energy and volume of flow units of metallic glasses. Scr. Mater. 67, 9-12.

Lu, Z., Shang, B.S., Sun, Y.T., Zhu, Z.G., Guan, P.F., Wang, W.H., Bai, H.Y., 2016. Revealing β-relaxation mechanism based on energy distribution of flow units in metallic glass. J. Chem. Phys. 144, 144501.

Luckabauer, M., Hayashi, T., Kato, H., Ichitsubo, T., 2019. Decreasing activation energy of fast relaxation processes in a metallic glass during aging. Phys. Rev. B 99, 140202.

Lüttich, M., Giordano, V.M., Le Floch, S., Pineda, E., Zontone, F., Luo, Y., Samwer, K., Ruta, B., 2018. Anti-Aging in Ultrastable Metallic Glasses. Phys. Rev. Lett. 120, 135504.

Lv, Z., Yuan, C., Ke, H., Shen, B., 2021. Defects activation in CoFe-based metallic glasses during creep deformation. J. Mater. Sci. Technol. 69, 42-47.

Ma, E., 2015. Tuning order in disorder. Nat. Mater. 14, 547-552.

Magagnosc, D.J., Kumar, G., Schroers, J., Felfer, P., Cairney, J.M., Gianola, D.S., 2014. Effect of ion irradiation on tensile ductility, strength and fictive temperature in metallic glass nanowires. Acta Mater 74, 165-182.

Méar, F.O., Lenk, B., Zhang, Y., Greer, A.L., 2008. Structural relaxation in a heavily cold-worked metallic glass. Scr. Mater. 59, 1243-1246.

Ngai, K., Wang, Z., Gao, X.Q., Yu, H.B., Wang, W.H., 2013. A connection between the structural α-relaxation and the β-relaxation found in bulk metallic glass-formers. J. Chem. Phys. 139, 014502.

Ngai, K.L., Capaccioli, S., 2004. Relation between the activation energy of the Johari-Goldstein beta relaxation and Tg of glass formers. Phys. Rev. E 69, 031501.

Ocelík, V., Csach, K., Kasardová, A., Bengus, V.Z., 1997. Anelastic deformation processes in metallic glasses and activation energy spectrum model. Mater. Sci. Eng., A 226-228, 851-855.

Packard, C.E., Homer, E.R., Al-Aqeeli, N., Schuh, C.A., 2010. Cyclic hardening of

metallic glasses under Hertzian contacts: Experiments and STZ dynamics simulations. Philos. Mag. 90, 1373-1390.

Pan, J., Ivanov, Y.P., Zhou, W.H., Li, Y., Greer, A.L., 2020. Strain-hardening and suppression of shear-banding in rejuvenated bulk metallic glass. Nature 578, 559-562.

Pan, J., Wang, Y.X., Guo, Q., Zhang, D., Greer, A.L., Li, Y., 2018. Extreme rejuvenation and softening in a bulk metallic glass. Nat. Commun. 9, 560.

Perez, J., 1990. Quasi-punctual defects in vitreous solids and liquid-glass transition. Solid State Ionics 39, 69-79.

Qiao, J.C., Wang, Q., Pelletier, J.M., Kato, H., Casalini, R., Crespo, D., Pineda, E., Yao, Y., Yang, Y., 2019. Structural heterogeneities and mechanical behavior of amorphous alloys. Prog. Mater. Sci. 104, 250-329.

Qiao, J.C., Wang, Y.-J., Zhao, L.Z., Dai, L.H., Crespo, D., Pelletier, J.M., Keer, L.M., Yao, Y., 2016. Transition from stress-driven to thermally activated stress relaxation in metallic glasses. Phys. Rev. B 94, 104203.

Qiao, J.C., Zhang, L.T., Tong, Y., Lyu, G.J., Hao, Q., Tao, K., 2022. Mechancial properties of amorphous alloys: In the framework of the microstructure heterogeneity. Adv. Mech. 52, 117-152.

Rao, W., Chen, Y., Dai, L.-H., 2022. A constitutive model for metallic glasses based on two-temperature nonequilibrium thermodynamics. Int. J. Plast. 154, 103309.

Ross, P., Küchemann, S., Derlet, P.M., Yu, H., Arnold, W., Liaw, P., Samwer, K., Maaß, R., 2017. Linking macroscopic rejuvenation to nano-elastic fluctuations in a metallic glass. Acta Mater 138, 111-118.

Song, L.J., Gao, M., Xu, W., Huo, J.T., Wang, J.Q., Li, R.W., Wang, W.H., Perepezko, J.H., 2020. Inheritance from glass to liquid: β relaxation depresses the nucleation of crystals. Acta Mater 185, 38-44.

Șopu, D., Moitzi, F., Mousseau, N., Eckert, J., 2020. An atomic-level perspective of shear band formation and interaction in monolithic metallic glasses. Applied Materials Today 21, 100828.

Spaepen, F., 1977. A microscopic mechanism for steady state inhomogeneous flow in

metallic glasses. Acta Metall. 25, 407-415.

Sun, Y., Concustell, A., Greer, A.L., 2016. Thermomechanical processing of metallic glasses: extending the range of the glassy state. Nat. Rev. Mater. 1, 16039.

Tanaka, H., 2004. Origin of the excess wing and slow β relaxation of glass formers: A unified picture of local orientational fluctuations. Phys. Rev. E 69, 021502.

Taub, A., Spaepen, F., 1981. Ideal elastic, anelastic and viscoelastic deformation of a metallic glass. J. Mater. Sci. 16, 3087-3092.

Tian, Z.-L., Wang, Y.-J., Chen, Y., Dai, L.-H., 2017. Strain gradient drives shear banding in metallic glasses. Phys. Rev. B 96, 094103.

Tong, Y., Dmowski, W., Bei, H., Yokoyama, Y., Egami, T., 2018. Mechanical rejuvenation in bulk metallic glass induced by thermo-mechanical creep. Acta Mater 148, 384-390.

Tong, Y., Iwashita, T., Dmowski, W., Bei, H., Yokoyama, Y., Egami, T., 2015. Structural rejuvenation in bulk metallic glasses. Acta Mater 86, 240-246.

Wang, B., Wang, L.J., Shang, B.S., Gao, X.Q., Yang, Y., Bai, H.Y., Pan, M.X., Wang, W.H., Guan, P.F., 2020. Revealing the ultra-low-temperature relaxation peak in a model metallic glass. Acta Mater 195, 611-620.

Wang, D.P., Qiao, J.C., Liu, C.T., 2019. Relating structural heterogeneity to β relaxation processes in metallic glasses. Mater. Res. Lett. 7, 305-311.

Wang, W.H., 2011. Correlation between relaxations and plastic deformation, and elastic model of flow in metallic glasses and glass-forming liquids. J. Appl. Phys. 110, 053521.

Wang, W.H., 2019. Dynamic relaxations and relaxation-property relationships in metallic glasses. Prog. Mater. Sci. 106, 100561.

Wang, X., Ruta, B., Xiong, L., Zhang, D., Chushkin, Y., Sheng, H., Lou, H., Cao, Q., Jiang, J., 2015. Free-volume dependent atomic dynamics in beta relaxation pronounced La-based metallic glasses. Acta Mater 99, 290-296.

Wang, X., Zhang, H., Douglas, J.F., 2021. The initiation of shear band formation in deformed metallic glasses from soft localized domains. J. Chem. Phys 155, 204504.

Wang, Y., Wei, Y., Zhao, Z., Long, H., Lin, Z., Guo, F., He, Q., Huang, C., Zhu, Y., 2022.

Activating dispersed strain bands in tensioned nanostructure layer for high ductility: The effects of microstructure inhomogeneity. Int. J. Plast. 149, 103159.

Wang, Z., Wang, W.-H., 2019. Flow units as dynamic defects in metallic glassy materials. Natl. Sci. Rev. 6, 304-323.

Wu, F.F., Zheng, W., Wu, S.D., Zhang, Z.F., Shen, J., 2011. Shear stability of metallic glasses. Int. J. Plast. 27, 560-575.

Yang, Q., Peng, S.-X., Wang, Z., Yu, H.-B., 2020. Shadow glass transition as a thermodynamic signature of β relaxation in hyper-quenched metallic glasses. Natl. Sci. Rev. 7, 1896-1905.

Yang, X.-S., Wang, Y.-J., Wang, G.-Y., Zhai, H.-R., Dai, L.H., Zhang, T.-Y., 2016a. Time, stress, and temperature-dependent deformation in nanostructured copper: Stress relaxation tests and simulations. Acta Mater 108, 252-263.

Yang, X.-S., Wang, Y.-J., Zhai, H.-R., Wang, G.-Y., Su, Y.-J., Dai, L.H., Ogata, S., Zhang, T.-Y., 2016b. Time-, stress-, and temperature-dependent deformation in nanostructured copper: Creep tests and simulations. J. Mech. Phys. Solids 94, 191-206.

Ye, J.C., Lu, J., Liu, C.T., Wang, Q., Yang, Y., 2010. Atomistic free-volume zones and inelastic deformation of metallic glasses. Nat. Mater. 9, 619-623.

Yu, H.-B., Samwer, K., 2014. Atomic mechanism of internal friction in a model metallic glass. Phys. Rev. B 90, 144201.

Yu, H.-B., Yang, M.-H., Sun, Y., Zhang, F., Liu, J.-B., Wang, C.Z., Ho, K.M., Richert, R., Samwer, K., 2018. Fundamental Link between β Relaxation, Excess Wings, and Cage-Breaking in Metallic Glasses. J. Phys. Chem. Lett. 9, 5877-5883.

Yu, H.B., Samwer, K., Wu, Y., Wang, W.H., 2012. Correlation between β relaxation and self-diffusion of the smallest constituting atoms in metallic glasses. Phys. Rev. Lett. 109, 095508.

Yu, H.B., Wang, W.H., Bai, H.Y., Samwer, K., 2014. The β-relaxation in metallic glasses. Natl. Sci. Rev. 1, 429-461.

Yu, H.B., Wang, W.H., Bai, H.Y., Wu, Y., Chen, M.W., 2010. Relating activation of shear transformation zones to β relaxations in metallic glasses. Phys. Rev. B 81, 220201.

Yu, H.B., Wang, W.H., Samwer, K., 2013. The β relaxation in metallic glasses: an overview. Mater, Today 16, 183-191.

Yuan, C., Lv, Z., Pang, C., Li, X., Liu, R., Yang, C., Ma, J., Ke, H., Wang, W., Shen, B., 2021. Ultrasonic-assisted plastic flow in a Zr-based metallic glass. Sci. China Mater. 64, 448-459.

Zhang, L., Duan, Y., Crespo, D., Pineda, E., Wang, Y., Pelletier, J.-M., Qiao, J., 2021. Dynamic mechanical relaxation and thermal creep of high-entropy $La_{30}Ce_{30}Ni_{10}Al_{20}Co_{10}$ bulk metallic glass. Sci. China: Phys., Mech. Astron. 64, 296111.

Zhang, Z., Wang, C., Liu, P., Reddy, K.M., Wang, X., Chen, M., Song, S., 2022. Deformation behavior of a nanoporous metallic glass at room temperature. Int. J. Plast. 152, 103232.

Zhu, F., Nguyen, H.K., Song, S.X., Aji, D.P.B., Hirata, A., Wang, H., Nakajima, K., Chen, M.W., 2016. Intrinsic correlation between β-relaxation and spatial heterogeneity in a metallic glass. Nat. Commun. 7, 11516.